

## Article

# Suppression of Harmonic Current in Magnetic Bearing–Rotor System with Redundant Structure

Baixin Cheng <sup>1,2</sup>, Xin Cheng <sup>1,2</sup>, Shao Song <sup>3</sup>, Rougang Zhou <sup>4,\*</sup> and Shuai Deng <sup>1,2</sup>

<sup>1</sup> School of Mechanical & Electronic Engineering, Wuhan University of Technology, Wuhan 430070, China; chengbaixin@126.com (B.C.); chengx@whut.edu.cn (X.C.); dengshuai2014@163.com (S.D.)

<sup>2</sup> Hubei Maglev Engineering Technology Research Center, Wuhan University of Technology, Wuhan 430070, China

<sup>3</sup> China Ship Development and Design Center, Wuhan 430070, China; songshao1986@126.com

<sup>4</sup> School of Mechanical Engineering, Hangzhou Dianzi University, Hangzhou 310000, China

\* Correspondence: zhourg@hdu.edu.cn; Tel.: +86-152-5715-4202

**Abstract:** The magnetic bearing–rotor system has the advantages of no mechanical friction and active vibration control. A magnetic bearing with redundant structures provides an effective method to apply fault-tolerant control to the magnetic bearing–rotor system. In this paper, in order to improve the robustness of a rotor suspended by a magnetic bearing with redundant structures, the harmonic current suppression approach is proposed. Firstly, the generation mechanism of harmonic current in the magnetic bearing–rotor system is analyzed. Secondly, on the basis of the current distribution theory of magnetic bearing with redundant structures, the linearization model of electromagnetic force is established. Then, the eight-pole symmetrical radial magnetic bearing is taken as the research object, and the control system model with a multi-excitation disturbance source is established under the condition of no coil failure. Lastly, considering the periodicity of disturbance signals, a repetitive controller that is suitable for magnetic bearing with redundant structures is proposed in this paper. Moreover, in order to verify the effectiveness of the proposed control strategy, we inserted the repetitive controller into the original controller applied to the magnetically levitated rotor with redundant structures, and the corresponding simulation was carried out. The results demonstrate that the repetitive control method proposed in this paper can effectively suppress the harmonic current and improve the suspension accuracy of the rotor supported by the magnetic bearing with redundant structures.

**Keywords:** magnetic bearings; redundant structures; harmonic current; repetitive control



**Citation:** Cheng, B.; Cheng, X.; Song, S.; Zhou, R.; Deng, S. Suppression of Harmonic Current in Magnetic Bearing–Rotor System with Redundant Structure. *Appl. Sci.* **2022**, *12*, 4126. <https://doi.org/10.3390/app12094126>

Academic Editors: José A. Tenreiro Machado, Jan Awrejcewicz, Hamed Farokhi, Roman Starosta, José M. Vega, Hari Mohan Srivastava and Ying-Cheng Lai

Received: 3 March 2022

Accepted: 13 April 2022

Published: 20 April 2022

**Publisher's Note:** MDPI stays neutral with regard to jurisdictional claims in published maps and institutional affiliations.



**Copyright:** © 2022 by the authors. Licensee MDPI, Basel, Switzerland. This article is an open access article distributed under the terms and conditions of the Creative Commons Attribution (CC BY) license (<https://creativecommons.org/licenses/by/4.0/>).

## 1. Introduction

Compared with mechanical bearings, magnetic bearings are considered to be superior with characteristics of no physical contact, low rotation friction, high speed, and long life. These advantages have led magnetic bearings to become the key components of important industrial fields, such as aero engines, turbine generators, and energy storage flywheels [1–3]. However, mechanical component damage and electrical part failure will render the system unable to continue working, and the rotor will fail. Therefore, the fault-tolerant design of magnetic bearings is an effective way to solve the problem that will improve the reliability of the magnetic-levitated bearing system while under extreme conditions [1,4,5].

On the basis of the strongly coupled fluxes and equivalent magnetic circuit model of the heteropolar magnetic bearing, Maslen and Meeker et al. first proposed magnetic bearings with redundant structures and designed the fault-tolerant control strategy when different coils fail [6]. The core of fault-tolerant control is to obtain the current distribution matrix and make the magnetic bearing generate the desired force with residual normal coils. Furthermore, the bias current linearization theory and current distribution matrix provide

an approach to achieve the fault-tolerant control for magnetic bearings with redundant structures. After the theory was proposed, related research was further carried out. Na and Palazzolo [7] proposed the Lagrange multiplier approach to obtain the current distribution matrix and analyzed the position stiffness and voltage stiffness of the magnetic bearing with redundant structures. They adopted the simulation and experiment to verify the validity of the fault-tolerant control strategy [8]. Moreover, Noh [9] established a fault-tolerant controller for the eight-pole symmetrical radial magnetic bearing with redundant structures and carried out an experiment on a turbo-molecular vacuum pump. They realized that the rotor remained levitated with the failure of three simultaneous coils at the rotor speed of 4200 rpm. Considering the magnetic leakage, eddy current, and reluctance of the ferromagnetic material path factors in the magnetic bearing, Na and Palazzolo [10–12] introduced a compensation coefficient to the force of magnetic bearing and obtained the corresponding current distribution matrix. Recently, Meeker [13] proposed an unbiased control theory to design a fault-tolerant controller for magnetic bearings with redundant structures, which can be applied to the encompassed bearings with an arbitrary number of poles. The current distribution matrix reflects the mapping relationship between electromagnetic force and current. Cheng and Cheng [14,15] extended the theory of calculating the current distribution matrix from the equilibrium position to nonequilibrium position and designed an improved fault-tolerant controller. The simulation results showed an improvement in the performance of the magnetic bearing–rotor system with the proposed fault-tolerant control strategy. For stators with the characteristics of an even number of evenly spaced poles of equal area, Meeker and Maslen [16] proposed an effectively simplified method to design a fault-tolerant controller while some coils fail in magnetic bearings. Different bias current coefficients can lead the magnetic bearing to produce different characteristics of electromagnetic force. Cheng and Deng [17] proposed an optimal algorithm to acquire the reasonable bias current coefficient, and the simulation results illustrated that the proposed approaches improve the system performance. Furthermore, according to the need of a fault-tolerant controller applied to magnetic bearings with redundant structures, they designed a fault-tolerant control scheme that includes dual DSP microprocessors and a power amplifier [18]. However, for magnetic bearings with redundant structures, most research has focused on obtaining the current distribution matrix when different coils fail. Nevertheless, there are several scientific questions that have been studied and solved in magnetic bearings under the differential control method.

For a rotor suspended with magnetic bearings under the differential control strategy, some advanced control methods have been applied to solve specific problems; a typical example is the mass unbalances of a rotor, and some researchers have proposed a series of approaches to suppress unbalanced rotor vibration. Mao et al. [19] designed a real-time variable step polygon iterative search algorithm that includes an unbalance compensator to suppress rotor vibration. Jian et al. [20] proposed an online unbalance compensation algorithm based on the least mean squares method and the influence coefficient method, and the experiment was carried out on a maglev rotor platform; the results demonstrated the effectiveness of the proposed control algorithm. In order to suppress the harmonic current of coils and rotor vibration produced by the mass unbalances and sensor runout, Cui et al. [21–24] analyzed the characteristics of the disturbance signal and proposed several repetitive controllers with different structures. Simulation and experimental results were given to show the superiority of proposed repetitive controllers. Moreover, to suppress the harmonic components in the full speed range, Cui [25] and He [26] proposed multiple phase-shift notch filters in series and in parallel modes. Moreover, in order to suppress the harmonic vibration of a magnetically suspended control moment gyro, Cui et al. [27] proposed a control algorithm that uses the orthogonal characteristics of the output signals of the  $x$ -direction and  $y$ -direction displacement sensors. The electromagnetic force of the magnetic bearing in a magnetically suspended control moment gyro was directly used as the input signal of the control to produce zero magnetic force control, and the experimental results demonstrated the validity of the algorithm. Jin [28] designed a

linear active disturbance rejection (LADRC) for magnetic bearings, and the experiments demonstrated that the LADRC had better anti-interference performance compared to the PID controller. Ran et al. [29] analyzed the dynamic characteristic of a flexible rotor suspended by magnetic bearings, and, according to the model of the system, the robust  $H_\infty$  controller was proposed. The experimental results indicated that the controller had superior performance of vibration suppression, enabling the flexible rotor to pass the first bending critical speed. Furthermore, Zhang et al. [30] proposed a nonlinear adaptive algorithm whose asymptotic stability is guaranteed by Lyapunov's theory to suppress the harmonics vibration of the magnetic bearing system. Using an unbalance suppression algorithm applied to piezoelectric active bearings for rotating machinery, Borquegallego et al. [31] presented a novel generalized notch filter for harmonic suppression control for magnetically levitated rotors, and the experimental results demonstrated that the control algorithm reduced the rotor in the level of generated vibrations by at least one order of magnitude. Sun et al. [32] proposed a modified iterative learning control including an extended state observer to suppress the disturbance of the hybrid magnetic bearing system, and the experimental results showed that the proposed strategy had better reference tracking and disturbance suppression ability than PID and neural network inverse control.

According to the aforementioned analysis, there has been no advanced control method studied for magnetic bearings with redundant structures. However, similar harmonic vibration exists in magnetic bearing systems with redundant structures. In this paper, magnetic bearings with redundant structures and no coil failure were considered as the research object. This paper proposed the inverse of the current distribution matrix  $W^{-1}$  used in the equivalent control closed-loop model with the current of each coil not being neglected. On the basis of the equivalent control model, the repetitive control is designed and applied to the system of magnetic bearings with redundant structures. The numerical results demonstrate that the proposed control scheme in this paper can not only suppress the harmonic current of each coil but also improve the robustness of the whole system.

The paper is organized as follows: the model of mass unbalance and sensor runout of is described in Section 2. The characteristics and control strategy of magnetic bearings with redundant structures are described, and the equivalent control closed-loop model is established in Section 3. The repetitive control (RC) is designed for magnetic bearings with redundant structures, and the simulation results are discussed in Section 4. Section 5 gives the conclusion.

## 2. Mode of Mass Unbalance and Sensor Runout

Periodic vibration is a typical problem in the system of a magnetically levitated rotor, and the vibration is mainly caused by the characteristics of the whole system. Therefore, it is necessary to analyze and express the motion characteristics and system noise of the structural parts of the system. In essence, the support between the magnetic bearing and rotor can be regarded as an elastic support with air gap. The mechanical structure uses its own material characteristics and mutual cooperation to form the electromagnetic field, and the electromagnetic force is formed between the rotor and the stator. The existence of machining error of the mechanical structure, uneven material, rotor imbalance, sensor noise, and nonlinear characteristics of each module of the control system can produce vibration with rich frequency components. Under the joint action of multisource vibration, the harmonic component disturbances of the fundamental and multiple frequencies are generated in the whole magnetic bearing–rotor system, and the current with the corresponding multi-frequency components is generated through the control system.

Uneven rotor mass is the main factor causing rotor vibration. Rotor unbalance mainly includes static imbalance and dynamic imbalance. Static unbalance refers to the deviation between the inertia axis center and the geometric axis center of the rotor. Dynamic unbalance means that the inertia axis of the rotor is different from the geometric axis.

The section of the single radial magnetic bearing–rotor system is shown in Figure 1. It is supposed that the geometric center plane of the rotor coincides with the inertial center

plane, and the geometric center of the rotor  $O_g$  is concentric with the geometric center of the magnetic bearing, The center of inertia of the rotor is  $O_i$ , and  $\varepsilon$  is the mass eccentricity. When the rotor rotates around the geometric center during operation, the unbalance forces  $F_{ex}$  and  $F_{ey}$  in the  $x$ - and  $y$ -directions can be expressed as

$$\begin{cases} F_{ex} = m\varepsilon\omega^2 \cos(\omega t + \zeta) \\ F_{ey} = m\varepsilon\omega^2 \sin(\omega t + \zeta), \end{cases} \quad (1)$$

where  $m$  is the mass of the rotor,  $\omega$  is the rotor speed, and  $\zeta$  is the initial phase.

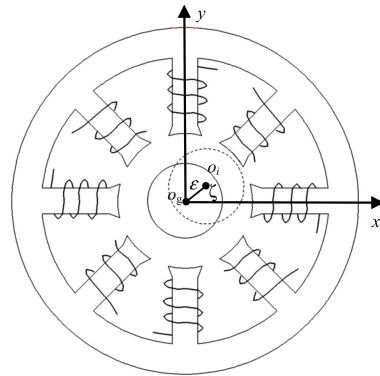


Figure 1. Section of single radial magnetic bearing-rotor system.

Due to the inevitable manufacturing errors in the rotor and stator of the magnetic bearing system shown in Figure 2, there is a lack of concentricity of the sensing surface and no uniform electrical or magnetic properties around the sensing surface. Therefore, while the rotor is in the process of rotation, the output signal of the displacement sensor contains the harmonic interference of synchronous and multiple frequencies of rotation speed. Thus, in a magnetically levitated rotor system with redundant structures, the signal of displacement sensors can be described as

$$\begin{cases} x_s = x_0 + x_d(t) \\ y_s = y_0 + y_d(t), \end{cases} \quad (2)$$

where  $x_d(t)$  and  $y_d(t)$  denote the sensor runout in the  $x$ - and  $y$ -directions of sensors, and the mathematical model can be described as

$$\begin{cases} x_d(t) = \sum_{i=1}^n a_{xi} \cos(i\omega t + \phi_{xi}) \\ y_d(t) = \sum_{i=1}^n a_{yi} \cos(i\omega t + \phi_{yi}) \end{cases}, i = 1, 2, \dots, n, \quad (3)$$

where  $i$  is the order of harmonics,  $a_{xi}$  and  $a_{yi}$  represent the sensor runout corresponding to the  $x$ - and  $y$ -direction sensors, and  $\phi_{xi}$  and  $\phi_{yi}$  are the initial phases.

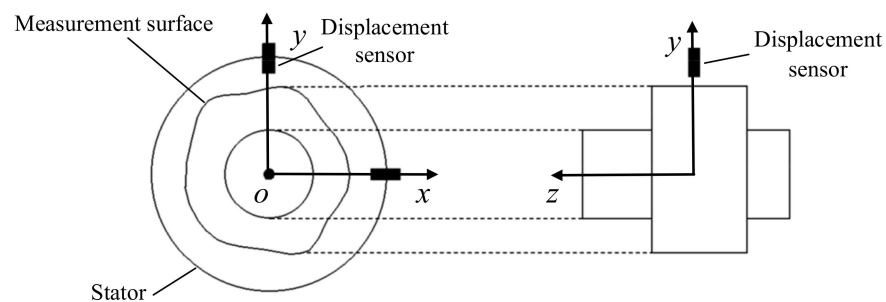


Figure 2. Mechanism diagram of sensor runout.

### 3. Characteristic and Control Strategy of Magnetic Bearings with Redundant Structures

Compared with magnetic bearings that adopt a differential control strategy, the coil of each pole is independent in magnetic bearings with  $n$ -pole heteropolar redundant structures. According to the mapping relationship between the electromagnetic forces and each pole of the magnetic bearing, a linear relationship between electromagnetic force and currents is constructed. Then, according to the inverse of the model, the current distribution controller can be designed. In this paper, an eight-pole symmetrical radial magnetic bearing was taken as the research object to illustrate the control strategy for magnetic bearings with redundant structures.

#### 3.1. Force Mode of Eight-Pole Magnetic Bearings with Redundant Structures

A radial magnetic bearing with eight-pole heteropolar redundant structures is depicted in Figure 3a, and the equivalent magnetic circuit model is illustrated in Figure 3b. The only sources of magnetic excitation in the bearing are the coils that are wound on each pole, and almost all circuit reluctance is due to the air gap associated with each pole.

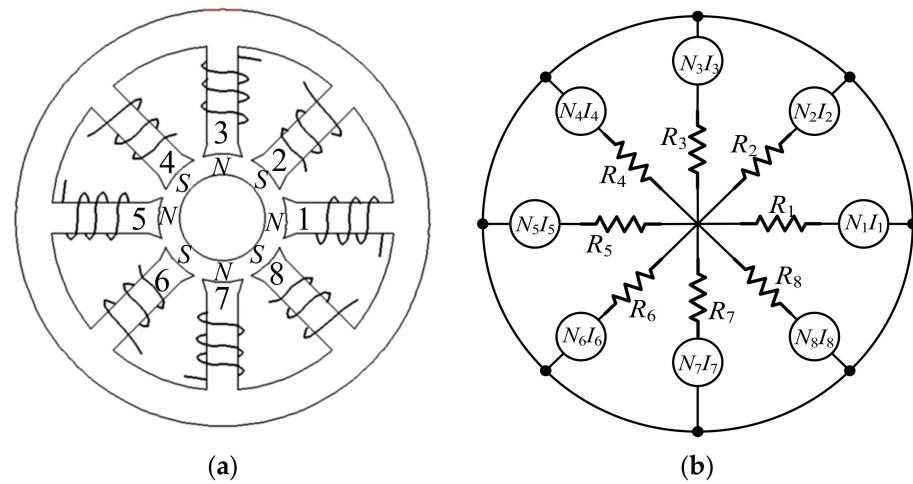


Figure 3. Eight-pole bearing arrangement (a) and equivalent magnetic circuit (b).

The relationship between the coil current and the magnetic flux can be written as

$$R_j \phi_j - R_{j+1} \phi_{j+1} = \bar{N}_j I_j - \bar{N}_{j+1} I_{j+1}, j = 1, 2, \dots, 8, \tag{4}$$

$$R_j = \frac{g_j}{\mu_0 A_j}, \tag{5}$$

where  $R_j$  is the reluctance of the  $j$ -th pole gap,  $g_j$  is the length of the  $j$ -th air gap,  $\mu_0$  is the permeability of vacuum,  $j$  is the number of poles, and  $A_j$ ,  $\phi_j$ ,  $\bar{N}_{j+1}$ , and  $I_j$  represent the area, magnetic flux, turns of the coil, and current in the  $j$ -th coil, respectively.

The air gap  $g_j$  is variable while the rotor deviates from its equilibrium position, and it can be described as follows [6]:

$$g_j = g_0 - x \cos \theta_j - y \sin \theta_j. \tag{6}$$

Meanwhile, the flux conservation is described as

$$\sum_{j=1}^n \phi_j = 0. \tag{7}$$

Therefore, Equation (4) can be rearranged as

$$\mathbf{R}\Phi = \bar{\mathbf{N}}\mathbf{I}. \tag{8}$$

Assuming that the magnetic flux density is uniform in the gap, the flux conservation can be described by Equation (9).

$$\Phi = AB, \tag{9}$$

where  $A$  is the diagonal matrix of the pole area, and  $B$  is the magnetic flux density matrix of the air gap, expressed as

$$B = A^{-1}R^{-1}\bar{N}I = VI. \tag{10}$$

The current distribution matrix  $W$  can be defined to describe the relationship between the current in each coil of the magnetic bearing and the logical control currents as shown in Equation (11).

$$W = [w_b, w_x, w_y],$$

$$I = W \begin{bmatrix} C_0 \\ i_x \\ i_y \end{bmatrix} = WI_c, \tag{11}$$

where  $C_0$  is the bias coefficient, and  $i_x$  and  $i_y$  are the logical control currents in the  $x$ - and  $y$ -directions, respectively. The resultant forces in the  $x$ - and  $y$ -directions can be described as

$$F_x(x, y) = I_c^T W^T M_x W I_c, \tag{12}$$

$$F_y(x, y) = I_c^T W^T M_y W I_c, \tag{13}$$

where

$$\begin{cases} M_x(x, y) = -V^T D_x V \\ M_y(x, y) = -V^T D_y V \\ D_x = \frac{A_j}{2\mu_0} \text{diag} [\cos \theta_j] \\ D_y = \frac{A_j}{2\mu_0} \text{diag} [\sin \theta_j] \end{cases}. \tag{14}$$

Furthermore, in order to ensure the linearization of the electromagnetic force, the current distribution matrix  $W(x, y)$  should be obtained to satisfy Equation (15).

$$\begin{cases} W^T(x, y)M_x W(x, y) - Q_x = 0 \\ W^T(x, y)M_y W(x, y) - Q_y = 0 \end{cases}, \tag{15}$$

where the matrices ( $Q_x$  and  $Q_y$ ) are defined as

$$Q_x = \begin{bmatrix} 0 & 0.5 & 0 \\ 0.5 & 0 & 0 \\ 0 & 0 & 0 \end{bmatrix}, Q_y = \begin{bmatrix} 0 & 0 & 0.5 \\ 0 & 0 & 0 \\ 0.5 & 0 & 0 \end{bmatrix}. \tag{16}$$

Through the calculation of the above theory, the electromagnetic forces can be linearized as

$$\begin{cases} F_x(x, y) = C_0 i_x \\ F_y(x, y) = C_0 i_y \end{cases}. \tag{17}$$

### 3.2. Stiffness of Magnetic Bearing with Redundant Structures

It is considered that the air gap between the poles and rotor is 0.4 mm while the rotor is at the equilibrium position, and the displacement of the rotor is tiny when the rotor is suspended by the magnetic bearing; thus, the electromagnetic force forms a linear relationship with the displacement and the logical control currents  $i_x$  and  $i_y$ . By using Taylor series expansion, the resultant forces in the  $x$ - and  $y$ -directions can be linearized as

$$F_x(x, y, i_x, i_y) \approx \frac{\partial F_x}{\partial x} \left. \begin{matrix} x = 0 \\ y = 0 \\ i_x = 0 \\ i_y = 0 \end{matrix} \right|_{x + \frac{\partial F_x}{\partial y}} \left. \begin{matrix} x = 0 \\ y = 0 \\ i_x = 0 \\ i_y = 0 \end{matrix} \right|_{y + \frac{\partial F_x}{\partial i_x}} \left. \begin{matrix} x = 0 \\ y = 0 \\ i_x = 0 \\ i_y = 0 \end{matrix} \right|_{i_x + \frac{\partial F_x}{\partial i_y}} \left. \begin{matrix} x = 0 \\ y = 0 \\ i_x = 0 \\ i_y = 0 \end{matrix} \right|_{i_y} \tag{18}$$

$$F_y(x, y, i_x, i_y) \approx \frac{\partial F_y}{\partial x} \left. \begin{matrix} x = 0 \\ y = 0 \\ i_x = 0 \\ i_y = 0 \end{matrix} \right|_{x + \frac{\partial F_y}{\partial y}} \left. \begin{matrix} x = 0 \\ y = 0 \\ i_x = 0 \\ i_y = 0 \end{matrix} \right|_{y + \frac{\partial F_y}{\partial i_x}} \left. \begin{matrix} x = 0 \\ y = 0 \\ i_x = 0 \\ i_y = 0 \end{matrix} \right|_{i_x + \frac{\partial F_y}{\partial i_y}} \left. \begin{matrix} x = 0 \\ y = 0 \\ i_x = 0 \\ i_y = 0 \end{matrix} \right|_{i_y} \tag{19}$$

$K_{xx}, K_{xy}, K_{yx},$  and  $K_{yy}$  are the position stiffness, and  $K_{i_{xx}}, K_{i_{xy}}, K_{i_{yx}},$  and  $K_{i_{yy}}$  are the current stiffness. On the basis of the nonlinear magnetic forces shown in Equations (12) and (13), the model of position stiffness can be presented as

$$-K_{xx} = \frac{\partial F_x}{\partial x} \left. \begin{matrix} x = 0 \\ y = 0 \\ i_x = 0 \\ i_y = 0 \end{matrix} \right|_{x + \frac{\partial F_x}{\partial y}} = \mathbf{w}_b^T \frac{\partial \mathbf{M}_x}{\partial x} \mathbf{w}_b C_0^2 \left. \begin{matrix} x = 0 \\ y = 0 \end{matrix} \right|_{y = 0} = \mathbf{w}_b^T \mathbf{M}_{xx0} \mathbf{w}_b C_0^2, \tag{20}$$

$$-K_{xy} = \frac{\partial F_x}{\partial y} \left. \begin{matrix} x = 0 \\ y = 0 \\ i_x = 0 \\ i_y = 0 \end{matrix} \right|_{x + \frac{\partial F_x}{\partial y}} = \mathbf{w}_b^T \frac{\partial \mathbf{M}_x}{\partial y} \mathbf{w}_b C_0^2 \left. \begin{matrix} x = 0 \\ y = 0 \end{matrix} \right|_{y = 0} = \mathbf{w}_b^T \mathbf{M}_{xy0} \mathbf{w}_b C_0^2, \tag{21}$$

$$-K_{yx} = \frac{\partial F_y}{\partial x} \left. \begin{matrix} x = 0 \\ y = 0 \\ i_x = 0 \\ i_y = 0 \end{matrix} \right|_{x + \frac{\partial F_y}{\partial y}} = \mathbf{w}_b^T \frac{\partial \mathbf{M}_y}{\partial x} \mathbf{w}_b C_0^2 \left. \begin{matrix} x = 0 \\ y = 0 \end{matrix} \right|_{y = 0} = \mathbf{w}_b^T \mathbf{M}_{yx0} \mathbf{w}_b C_0^2, \tag{22}$$

$$-K_{yy} = \frac{\partial F_y}{\partial y} \left. \begin{matrix} x = 0 \\ y = 0 \\ i_x = 0 \\ i_y = 0 \end{matrix} \right|_{x + \frac{\partial F_y}{\partial y}} = \mathbf{w}_b^T \frac{\partial \mathbf{M}_y}{\partial y} \mathbf{w}_b C_0^2 \left. \begin{matrix} x = 0 \\ y = 0 \end{matrix} \right|_{y = 0} = \mathbf{w}_b^T \mathbf{M}_{yy0} \mathbf{w}_b C_0^2. \tag{23}$$

The model of current stiffness can be calculated as

$$K_{i_{xx}} = \frac{\partial F_x}{\partial I_c} \frac{\partial I_c}{\partial i_x} \left. \begin{matrix} x = 0 \\ y = 0 \\ i_x = 0 \\ i_y = 0 \end{matrix} \right| = \mathbf{w}_x^T \mathbf{M}_x \mathbf{w}_b C_0 + \mathbf{w}_b^T \mathbf{M}_x \mathbf{w}_x C_0 \left. \begin{matrix} x = 0 \\ y = 0 \end{matrix} \right|, \quad (24)$$

$$K_{i_{xy}} = \frac{\partial F_x}{\partial I_c} \frac{\partial I_c}{\partial i_y} \left. \begin{matrix} x = 0 \\ y = 0 \\ i_x = 0 \\ i_y = 0 \end{matrix} \right| = \mathbf{w}_y^T \mathbf{M}_x \mathbf{w}_b C_0 + \mathbf{w}_b^T \mathbf{M}_x \mathbf{w}_y C_0 \left. \begin{matrix} x = 0 \\ y = 0 \end{matrix} \right|, \quad (25)$$

$$K_{i_{yx}} = \frac{\partial F_x}{\partial I_c} \frac{\partial I_c}{\partial i_y} \left. \begin{matrix} x = 0 \\ y = 0 \\ i_x = 0 \\ i_y = 0 \end{matrix} \right| = \mathbf{w}_x^T \mathbf{M}_y \mathbf{w}_b C_0 + \mathbf{w}_b^T \mathbf{M}_y \mathbf{w}_x C_0 \left. \begin{matrix} x = 0 \\ y = 0 \end{matrix} \right|, \quad (26)$$

$$K_{i_{yy}} = \frac{\partial F_x}{\partial I_c} \frac{\partial I_c}{\partial i_y} \left. \begin{matrix} x = 0 \\ y = 0 \\ i_x = 0 \\ i_y = 0 \end{matrix} \right| = \mathbf{w}_y^T \mathbf{M}_y \mathbf{w}_b C_0 + \mathbf{w}_b^T \mathbf{M}_y \mathbf{w}_y C_0 \left. \begin{matrix} x = 0 \\ y = 0 \end{matrix} \right|. \quad (27)$$

According to the above analysis, the decoupled linearized magnetic forces can be expressed with position stiffness and current stiffness, and they can be used to design a control law to ensure the stability of the system.

### 3.3. Control Strategy and Analysis of Magnetic Bearings with Redundant Structures

The essence of the current distribution matrix  $\mathbf{W}$  is the mapping relationship between the logic currents and the current of each coil. The current distribution control strategy is designed with the mapping relationship described in Equation (10), and the distribution control strategy can be treated as a part of the system control strategy in the magnetic bearing with redundant structures. The entire system controller is described in Figure 4.

In Figure 4, the system controller includes the PID controller and current distribution controller. According to the error between the desired rotor position signal and the feedback of the actual rotor position, the PID algorithm controls the rotor position. With the control strategy described in Figure 4, the electromagnetic forces of the rotor while at the equilibrium position can be considered as a linear relationship with displacement and logic current. For a deep analysis of the relationship between logic control current and current of each coil in the magnetic bearing, we can use the inverse of the current distribution

matrix and current of each coil to form the logic control current; this relationship can be described as

$$I_c = W^{-1}I. \tag{28}$$

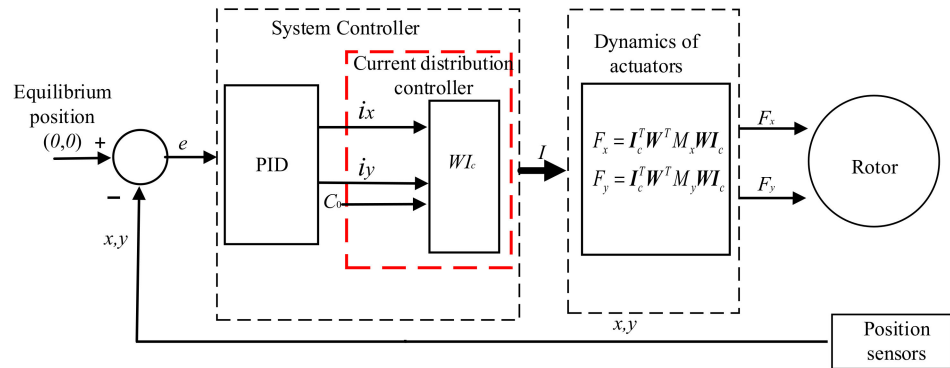


Figure 4. Closed-loop control strategy in magnetic bearings with redundant structures.

In this paper, the structural parameters of the eight-pole symmetrical radial magnetic bearing are shown in Table 1. The corresponding current distribution matrix  $W$  is

$$W = \frac{g_0}{4N\sqrt{\mu_0 A}} \begin{bmatrix} 2 & 2 & 0 \\ -2 & -\sqrt{2} & -\sqrt{2} \\ 2 & 0 & 2 \\ -2 & \sqrt{2} & -\sqrt{2} \\ 2 & -2 & 0 \\ -2 & \sqrt{2} & \sqrt{2} \\ 2 & 0 & -2 \\ -2 & -\sqrt{2} & \sqrt{2} \end{bmatrix}. \tag{29}$$

Table 1. Structural parameters of magnetic bearing.

Structure Parameter	Value	Unit
Pole area, $A_0$	$5.4 \times 10^{-5}$	$m^2$
Turns per coil, $\bar{N}$	56	/
Pole initial gap, $g_0$	$4 \times 10^{-4}$	m
Pole angle, $\theta_j$	$(j - 1)\pi/4$	rad
Saturation magnetic-flux density, $B_{sat}$	1.2	T
Rotor weight, $m$	0.8	kg

On the basis of the structural parameters of the magnetic bearing and current distribution matrix, the position stiffness and current stiffness can be calculated using Equations (20)–(27), where  $K_{xx} = -40,000$  N/m,  $K_{xy} = K_{yx} = 0$ ,  $K_{yy} = -40,000$  N/m,  $K_{ix} = 4$  A/m,  $K_{ixy} = K_{iyx} = 0$ , and  $K_{iyy} = 4$  A/m. The results show that the essence of the bias current coefficient is current stiffness. For the eight-pole symmetrical radial magnetic bearing studied in this paper, the electromagnetic forces can also be described as

$$\begin{aligned} F_x &= -K_{xx}x + K_{ixx}i_x \\ F_y &= -K_{yy}y + K_{iyy}i_y \end{aligned} \tag{30}$$

Furthermore, considering the unbalanced force and neglecting the torque of the rotor, the rotor dynamic equation in the  $x$ - and  $y$ -directions can be written as

$$\begin{aligned} m\ddot{x} &= F_x + F_{ex} \\ m\ddot{y} &= F_y + F_{ey} \end{aligned} \tag{31}$$

Through the above analysis, the equivalent control schematic diagram of the entire system can be depicted as shown in Figure 5.

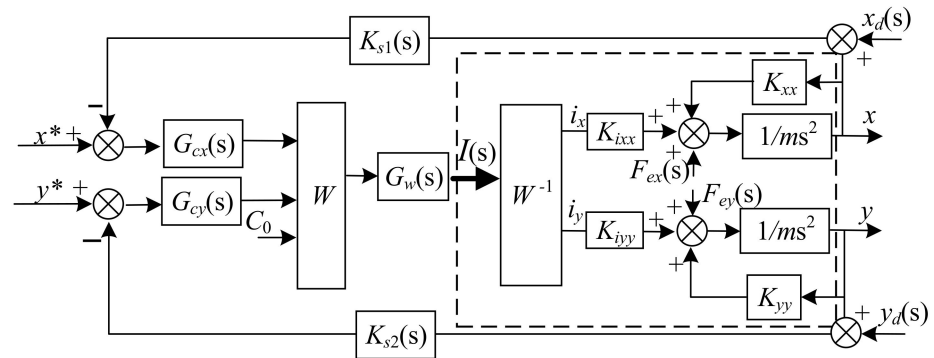


Figure 5. Closed-loop equivalent control schematic diagram of the entire system.

As shown in Figure 5,  $x^*$ ,  $y^*$ ,  $i_x^*$ , and  $i_y^*$  denote the desired position and desired logic control current, respectively.  $G_{cx}$  and  $G_{cy}$  are the position control law in the  $x$ - and  $y$ -directions;  $G_w$  is the transfer function of the amplifier, where  $G_w = 1 \text{ A/V}$ ;  $K_{sx}$  and  $K_{sy}$  are the gain of sensors.  $I(s)$  denotes the current of each coil in magnetic bearing. From Figure 5, although the currents in the coils determine the displacement of the rotor in both  $x$ - and  $y$ -directions, in view of the logic control current, the motion of the rotor in the  $x$ - and  $y$ -directions can be considered decoupled. Therefore, the equivalent control schematic diagram in the  $x$ -direction can be described as shown in Figure 6.

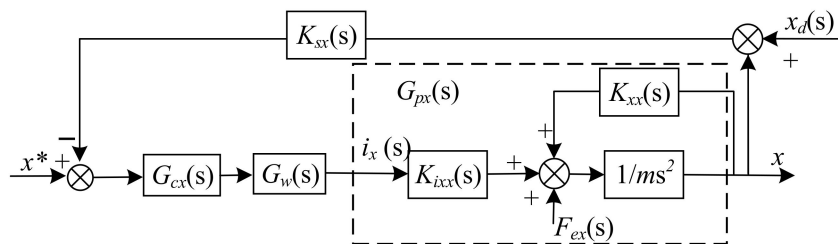


Figure 6. Equivalent control schematic diagram in the  $x$ -direction.

According to Figure 6, the logic current  $i_x(s)$  influenced by the unbalance force and sensor runout can be described as

$$i_x(s) = \frac{G_{cx}(s)G_w(s)}{1+K_{sx}(s)G_{cx}(s)G_w(s)G_{px}(s)}x^* + \frac{-K_{sx}(s)G_{cx}(s)G_w(s)}{1+K_{sx}(s)G_{cx}(s)G_w(s)G_{px}(s)}x_d(s) + \frac{-K_{sx}(s)G_{cx}(s)G_w(s)G_{px}(s)}{K_{ixx}(s)[1+K_{sx}(s)G_{cx}(s)G_w(s)G_{px}(s)]}F_{ex}(s) \tag{32}$$

From Equation (32), it can be concluded that the unbalance force  $F_{ex}$  and sensor runout  $x_d$  will induce the logic harmonic  $i_x$ . Logic current reflects the harmonic characteristics of current in the coils, which will cause undesirable multifrequency vibration of the rotor. If not suppressed, the vibration caused by unbalance mass and sensor runout will degrade the system performance and even lead to system instability. In a magnetic bearing–rotor system with redundant structures, to achieve the purpose of suppressing current harmonics, it is necessary to add the corresponding method in the control loop of the  $x$ - and  $y$ -directions at the same time.

#### 4. Suppression of Harmonic Current in AMB with Redundant Structures

The idea of repetitive control (RC) is derived from the internal model principle of control theory. In essence, repetitive control uses the periodic compensation of errors to realize the tracking of the desired signal and suppression of disturbance signals. According

to the characteristics of the disturbance signals occurring in the magnetic bearing–rotor system, repetitive controllers can effectively suppress harmonic currents. Furthermore, the design of the repetitive controller can be independent of the design of the original system controller. For a system that does not include a repetitive controller, there is no need to make any changes to the original system parameters; one can simply insert the repetitive controller into the original system and ensure that the new system meets the stability conditions.

4.1. Analysis of Magnetic Bearing System with RC

Taking the control loop of the magnetic bearing–rotor system in the  $x$ -direction as an example, the repetitive controller  $G_{xRC}$  is added into the original system. The control block diagram with RC is depicted in Figure 7, where  $Q(s)$  is the low-pass filter,  $C(s)$  is the phase compensator for the middle and low frequencies, the phase compensator  $e^{-T_2s}$  is used for high frequency,  $e^{-T_1s}$  is the time delay element,  $K_{rc}$  is the gain of RC and ensures the robustness of the system,  $T_1 + T_2 = T = 1/f$ , and  $f$  is the fundamental frequency of the disturbance signal.

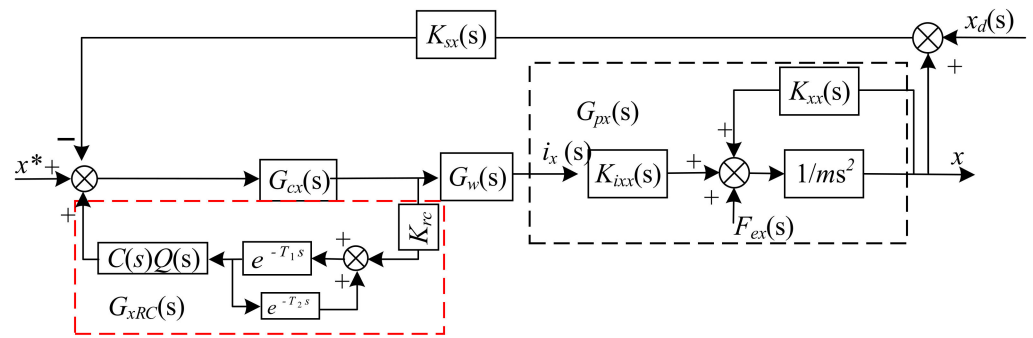


Figure 7. Control schematic diagram in  $x$ -direction with RC.

The transfer function of the proposed RC can be expressed as

$$G_{xRC}(s) = \frac{e^{-T_1s}}{1 - e^{-(T_1+T_2)s}} Q(s) K_{rc}(s) C(s). \tag{33}$$

$S_0$  is the sensitivity function of the system without RC, and it can be expressed as

$$S_0(s) = \frac{G_c(s)G_w(s)}{1 + G_c(s)G_w(s)G_p(s)K_s(s)}. \tag{34}$$

The logical current  $i_x$  is as the virtual output of the magnetic bearing, according to Figure 7. The logical current  $i_x$  can be written as

$$i_x(s) = \frac{S_0(s)[1 - e^{-Ts}][R(s) - D(s)K(s)]}{1 - e^{-Ts} - K_{rc}C(s)Q(s)\frac{S_0(s)}{G_w(s)}e^{-T_1s}}. \tag{35}$$

While the frequency  $w$  of disturbance signal is lower than the cut-off frequency  $w_c, w = \frac{2\pi}{T}n$  ( $n = 1, 2, 3, \dots$ ). Obviously, according to Euler’s formula, we can conclude that  $|e^{-Ts}|_{s=jw} = 1$  and  $\arg[e^{-Ts}]_{s=jw} = -2n\pi$ ; therefore,

$$1 - e^{-Ts} = 0. \tag{36}$$

Equation (36) denotes that the proposed RC can eliminate the disturbances which consist of multiples of the fundamental frequency  $f$ . However, the system with the RC

should satisfy the stability conditions of the system. The transfer function of the whole system is

$$G(s) = \frac{G_{cx}(s)G_w(s)G_p(s)}{1 - G_{cx}(s)G_{xRC}(s) + G_{cx}(s)G_w(s)G_p(s)K_s(s)}. \tag{37}$$

The closed-loop characteristic equation can be obtained as

$$1 - G_{cx}(s)G_{xRC}(s) + G_{cx}(s)G_w(s)G_p(s)K_{s1}(s) = 0. \tag{38}$$

Equation (38) can be rearranged as

$$M(s) - e^{-T_s s}N(s) = 0, \tag{39}$$

where

$$\begin{aligned} M(s) &= 1 + G_c(s)G_w(s)G_p(s)K_s(s), \\ N(s) &= 1 + G_c(s)K_{rc}C(s)Q(s)e^{T_2 s} + G_c(s)G_w(s)G_p(s)K_s(s). \end{aligned}$$

The regeneration spectrum of the whole system can be obtained as

$$R(\omega) = \left| \frac{N(s)}{M(s)} \right|_{s=j\omega} = \left| 1 + K_{rc}C(s)Q(s)e^{T_2 s} \times \frac{G_c(s)}{1 + G_c(s)G_w(s)G_p(s)K_s(s)} \right|_{s=j\omega}. \tag{40}$$

Generally, a smaller value of the regeneration spectrum function denotes better relative stability of the system. According to the small gain theory, the sufficient condition of the closed-loop system depicted in Figure 7 is given by

(1)  $F(s) = \frac{G_c(s)}{1 + G_c(s)G_w(s)G_p(s)K_s(s)}$  is stability, (2)  $R(\omega) < 1$ .

It is assumed that the original system is stable, and that the system has met condition 1. Therefore, the structure of the repetitive controller needs to be designed to make the system meet condition 2. Hence, we assume that  $\omega < \omega_c$ , and we define  $F(s)|_{s=j\omega} = A(\omega)e^{j\theta(\omega)}$ ,  $C(s)|_{s=j\omega} = B(\omega)e^{j\theta_c(\omega)}$ , and  $\beta(\omega) = \theta(\omega) + \theta_c(\omega) + T_2\omega$ ,  $T_2 = N_2T_s$ , where  $N_2$  is an integer and  $T_s$  is the sampling period of the system. Combining Equation (40) with condition 2, we obtain

$$\left| 1 + K_{rc}B(\omega)A(\omega)e^{j[\theta(\omega) + \theta_c(\omega) + T_2\omega]} \right|_{s=j\omega} < 1. \tag{41}$$

Then,

$$|1 + K_{rc}B(\omega)A(\omega)\cos\beta(\omega) + jK_{rc}B(\omega)A(\omega)\sin\beta(\omega)|_{s=j\omega} < 1. \tag{42}$$

Furthermore, we get

$$2K_{rc}B(\omega)A(\omega)\cos\beta(\omega) + [K_{rc}B(\omega)A(\omega)]^2 < 0. \tag{43}$$

The stability of the system with RC can be guaranteed, if the following condition is satisfied:

$$\begin{cases} 90^\circ < \beta(\omega) < 270^\circ \\ K_{rc} < \frac{2\min|\cos\beta(\omega)|}{\max[A(\omega)B(\omega)]} \end{cases}. \tag{44}$$

#### 4.2. Design of the RC for AMB with Redundant Structures

In this paper, as shown in Figure 7,  $K_{sx} = 5000$  V/m,  $T_s = 0.0002$  s, and  $G_w = 1$  A/V were defined. The transfer functions of the controllers  $G_{cx}$  and  $G_{px}$  are described as

$$G_{cx}(s) = k_p + \frac{k_i}{s} + k_d s, \tag{45}$$

$$G_{px}(s) = \frac{K_{ixx}}{ms^2 - K_{xx}}, \tag{46}$$

where  $k_p = 10$ ,  $k_i = 4$ , and  $k_d = 0.01$ .

Considering the mode of the magnetic bearing with redundant structures and control system, the phase–frequency characteristic curve of the  $F(s)$  is presented in Figure 8, and it is shown that the phase is below  $90^\circ$  in the middle- and high-frequency range. Hence, the phase  $\theta(\omega)$  of the  $F(s)$  does not satisfy the stability requirement. In order to solve the problem, we can design the repetitive controller to adjust the phase of the entire system.

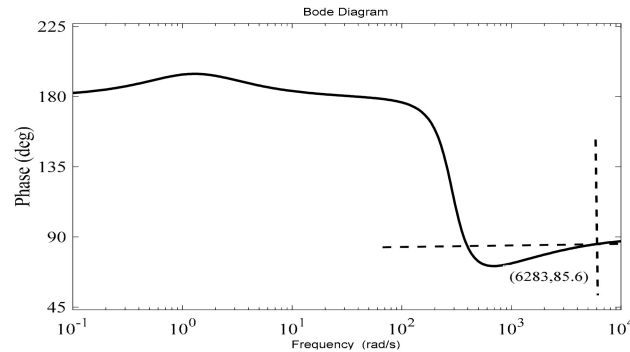


Figure 8. Phase–frequency diagram of  $F(s)$ .

(1) Design of low-pass filter  $Q(s)$

The main function of the low-pass filter (LPF) is to ensure the cutoff frequency of the system and eliminate the influence of high-frequency interference components that are applied to the entire system. To avoid the harmonic disturbance in the low-frequency region, the gain of the low-pass filter is usually required to be 0 dB, and the phase of the low-pass filter is required to be zero so as to ensure that the system is stable.

Assuming a rotor speed of 60 Hz, and considering that the first, second, third, and fourth harmonic currents are required to be suppressed, the cutoff frequency of the low-pass filter was chosen as 1000 Hz. The conventional LPF is usually designed as  $Q_1(s) = \frac{1}{0.0000159s+1}$ . However, this will lead to phase delay in the repetitive controller loop and degrade the performance of the system. To avoid this problem, a zero-phase low-pass filter was designed to replace the conventional LPF. Considering the cutoff frequency of the system, the zero-phase LPF was designed as follows:

$$Q(z) = 0.212z + 0.575 + 0.212z^{-1}. \tag{47}$$

In Figure 9, the blue and red lines indicate the amplitude and phase curve of the zero-phase low-pass filter and conventional LPF, respectively. By comparing the characteristics of  $Q(z)$  and  $Q_1(z)$ , the following conclusions can be drawn: for a conventional LPF, although the gain is 0 dB, the phase changes in the middle- and high-frequency domain, but there is no phase change for the zero-phase low-pass filter. Hence, we adopted the zero-phase low-pass filter shown in Equation (47).

(2) Design of phase compensator of  $F(s)$

According to the analysis of the previous sections, the phase compensator  $e^{T_2s}$  was used to improve the performance of  $F(s)$  in the high-frequency domain, and the  $C(s)$  was designed to compensate for the phase of the transfer function  $F(s)$  in the middle-frequency band.

(a) Design of  $e^{T_2s}$  for  $F(s)$  in high-frequency domain

For the magnetically levitated rotor with redundant structures in this paper, in order to suppress the noise of the system below the cutoff frequency, the phase–frequency characteristics in  $(0, 6283)$  rad/s should be considered. As shown in Figure 8,  $\theta(\omega) = 86.5^\circ$

when the frequency is 6283 rad/s. Thus, in order to satisfy Equations (44),  $e^{T_2s}$  should meet the following criterion:

$$4.4^\circ < T_2\omega|_{\omega=\omega_c} < 184.4^\circ, (T_2 = N_2T_s). \tag{48}$$

The sampling time  $T_s = 0.0002$  s, and  $N_2$  can be chosen as 1 or 2. The phase responses of  $\beta(\omega)$  with different  $N_2$  are shown in Figure 10. Obviously, when  $N_2$  was set to 1 or 2, the phase  $\theta(\omega)$  at  $\omega_c$  was changed to about  $150^\circ$  or  $230^\circ$ . This result indicates that the system satisfies the stability condition. Considering sufficient stability margin of the system, the value of  $N_2$  was selected as 1.

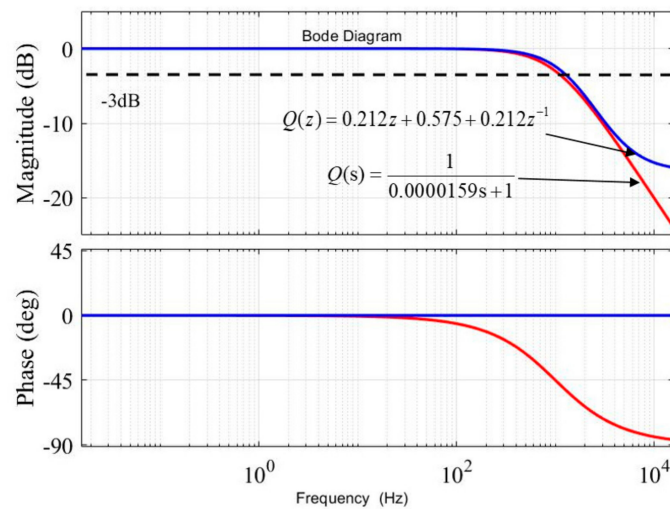


Figure 9. Bode plot of  $Q(z)$  with different filters.

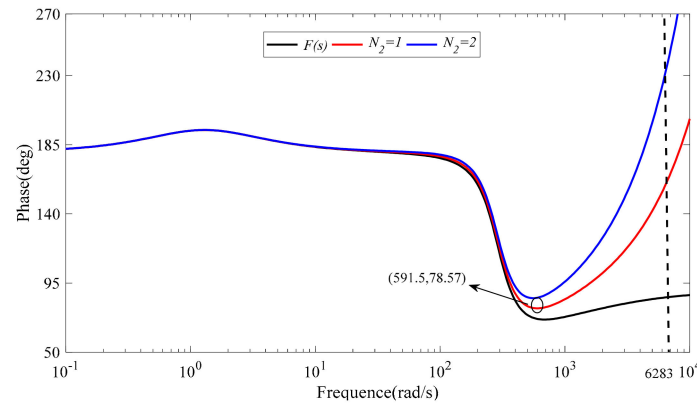


Figure 10. Bode plot of  $F(s)e^{T_2s}$ .

(b) Design of  $C(s)$  for  $F(s)$  in the middle-frequency domain

Although, by inserting  $e^{T_2s}$ , the phase characteristic of  $e^{T_2s}F(s)$  in the high-frequency domain is compensated for and improved, as shown in Figure 10, the value of the phase is still unchanged and below  $90^\circ$  in the middle-frequency domain; thus, the phase lag  $e^{T_2s}F(s)$  in the middle-frequency domain will lead to system instability. Therefore, it is necessary to design the phase compensator to improve the phase characteristic of the system in the middle-frequency range. To avoid the insertion of the phase lead compensator affecting the phase in the high-frequency range, the phase lead and phase lag were combined to form the phase compensator  $C(s)$  as

$$C(s) = \frac{0.0015s + 1}{0.00526s + 1} \bullet \frac{0.0068s + 1}{0.00051s + 1}. \tag{49}$$

After introducing the phase compensator  $C(s)$ , the phase–frequency curve is as shown in Figure 11.

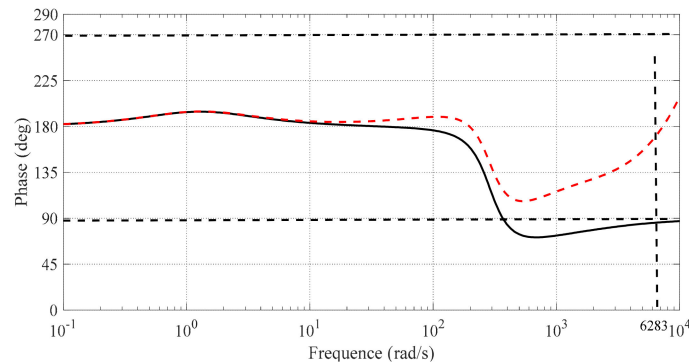


**Figure 11.** Phase–frequency curve of  $F(s)$  (black line) and  $C(s)F(s)$  (red dotted line).

As shown in Figure 11, the black line denotes the phase–frequency characteristic of  $F(s)$ , and the red dotted line denotes the phase–frequency characteristic of  $C(s)F(s)e^{T_2s}$ . It can be observed that the phase range was about  $(100^\circ, 175^\circ)$  within  $(0, \omega_c)$ . Thus, it can be seen that, when the phase compensator  $e^{T_2s}$  and  $C(s)$  are applied in the system, Equation (44) is satisfied.

(3) Design of fractional delay filters

In practice, the repetitive controller generally is adopted in discrete form. The discrete form of delay  $e^{-T_1s}$  in repetitive control is  $z^{-N}$ , and  $N$  is an integer. It depends on the ratio of the sampling frequency  $f_s$  to the fundamental frequency  $f$ . The value of  $f_s$  is usually fixed, and it is possible to make the value of  $N$  a non-integer for sampling frequency  $f_s$  with different values. In this paper, fundamental frequency  $f = 60$  Hz, sampling frequency  $f_s = 5000$  Hz, and  $N = 83.333$ . To solve this problem, Lagrange interpolation-based fractional delay (FD) filters were adopted to approximate the fractional part. For the standard fractional delay function  $H_F(z) = z^{-F}$ , it can be described as

$$H_F(z) \approx \sum_{n=0}^{N_m} h(z)z^{-n}$$

$$h(z) = \prod_{\substack{k=0 \\ k \neq n}}^{N_m} \frac{z-k}{n-k}, (n = 0, 1 \dots N_n) \tag{50}$$

In this paper, because  $N_2 = 1$  and  $N_1 = N - N_2 = 82.333$ , the discrete form of  $e^{-T_1s}$  can be written as  $z^{-82.333}$ , which can be divided into integer and decimal parts, i.e.,  $z^{-82.333} = z^{-81} \times z^{-1.333}$ . According to Equation (50) and  $N_m = 3$ , we can obtain  $h(0) = -0.0617, h(1) = 0.7411, h(2) = 0.3699$ , and  $h(3) = -0.0493$ . Therefore,  $z^{-1.333}$  can be rewritten as

$$z^{-1.333} \approx h(0) + h(1)z^{-1} + h(2)z^{-2} + h(3)z^{-3}. \tag{51}$$

Furthermore, according to Equation (44),  $K_{rc} = 0.001$  in this paper. Accordingly, combining the designed modules, the structure of the proposed repetitive controller for the magnetically suspended rotor with redundant structures in the  $x$ -direction can be depicted as in Figure 12.

4.3. Simulation Verification and Analysis

In order to verify the effectiveness of the proposed control strategy, simulations on the magnetic bearing–rotor system with redundant structures were carried out on Matlab/Simulink. The repetitive controller was designed according to the loop model of the equivalent control system shown in Figure 7. The currents of the coils were determined by the  $x$  and  $y$  control loops in the maglev bearing–rotor system. On the basis of the

closed-loop equivalent control schematic diagram of the entire system shown in Figure 5, we established the control structure shown in Figure 13.  $G_{xRC}(s)$  and  $G_{yRC}(s)$  represent the repetitive controllers applied to the  $x$ - and  $y$ -directions, respectively. Considering the symmetry of the magnetic bearing, we defined the structure of  $G_{yRC}(s)$  as the same as  $G_{xRC}(s)$ , and that of  $G_{cx}(s)$  as the same as  $G_{cy}(s)$ .

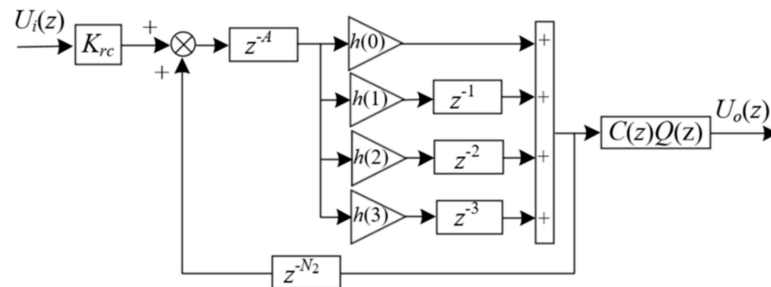


Figure 12. Structure of proposed repetitive controller in this paper.

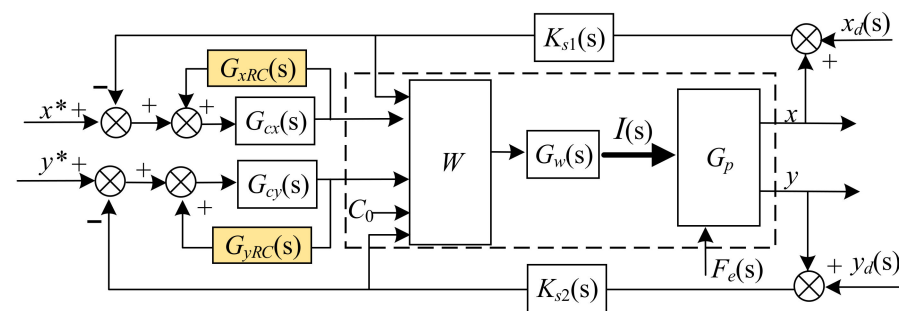


Figure 13. Control block diagram of the entire system with repetitive controllers.

However, there was a phase lead link  $z$  in the zero-phase LPF, and it could not be used directly in the Simulink platform. To solve this problem, we took an approximate approach to replace  $z$ . For this paper, the continuous model of  $z$  was  $e^{0.0002s}$ , which could be approximately expressed as

$$e^{0.0002s} \approx 1 + 0.0002s + \frac{1}{2}(0.0002)^2s^2. \tag{52}$$

The phase frequency characteristic curves of  $e^{0.0002s}$  and  $1 + 0.0002s + \frac{1}{2}(0.0002)^2s^2$  are expressed by red line and dotted blue line, respectively, in Figure 14, revealing a very small error between the two curves for frequencies below the cutoff frequency. Therefore, we used  $1 + 0.0002s + \frac{1}{2}(0.0002)^2s^2$  to replace  $e^{0.0002s}$  in the Simulink platform.

In order to ensure the validity of the disturbance signal, we obtained the date of the displacement sensor from the experimental platform as shown in Figure 15.

As shown in Figure 15, perturbation information can be considered within the sixth harmonic, and the parameters of mass unbalance and sensor runout are given in Table 2. Additionally, we assumed that the mode of sensor runout  $y_d(s)$  was the same as  $x_d(s)$ .

In order to demonstrate the advantages of introducing the repetitive controller to effectively suppress the harmonic disturbance of the system, the transient response of currents in the time domain in each coil before and after applying the repetitive controller is displayed in Figure 16. It should be noted that the positive and negative currents result in the poles of the magnetic bearing producing different magnetic field (NSN . . . NS), which is a typical characteristic of a heteropolar magnetic bearing with redundant structures when no coil fails.

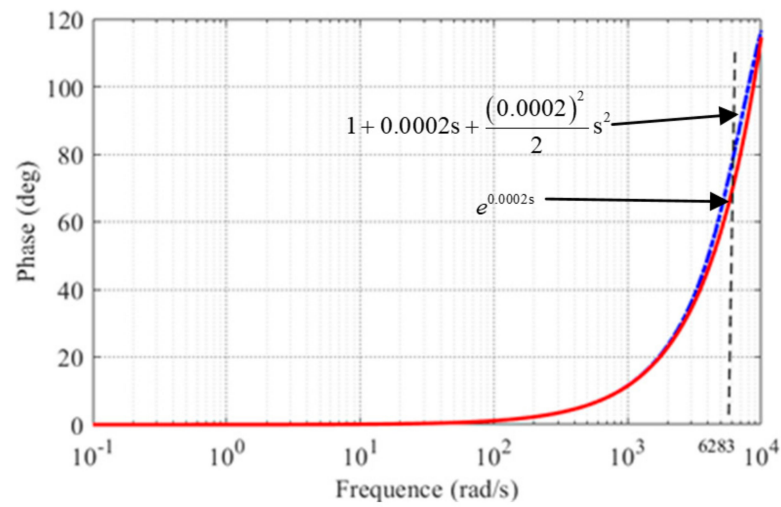


Figure 14. Phase–frequency characteristics of  $e^{0.0002s}$  and  $1 + 0.0002s + \frac{1}{2}(0.0002)^2s^2$ .

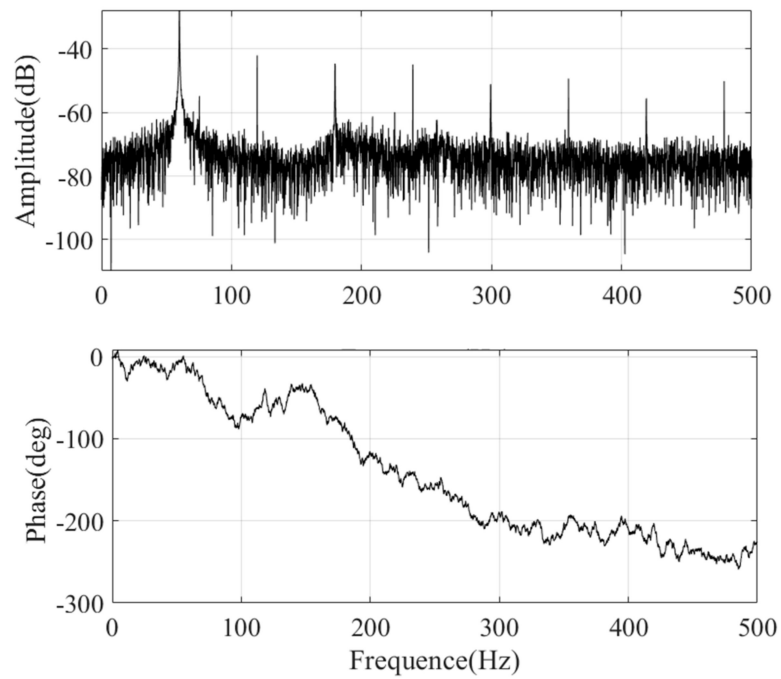
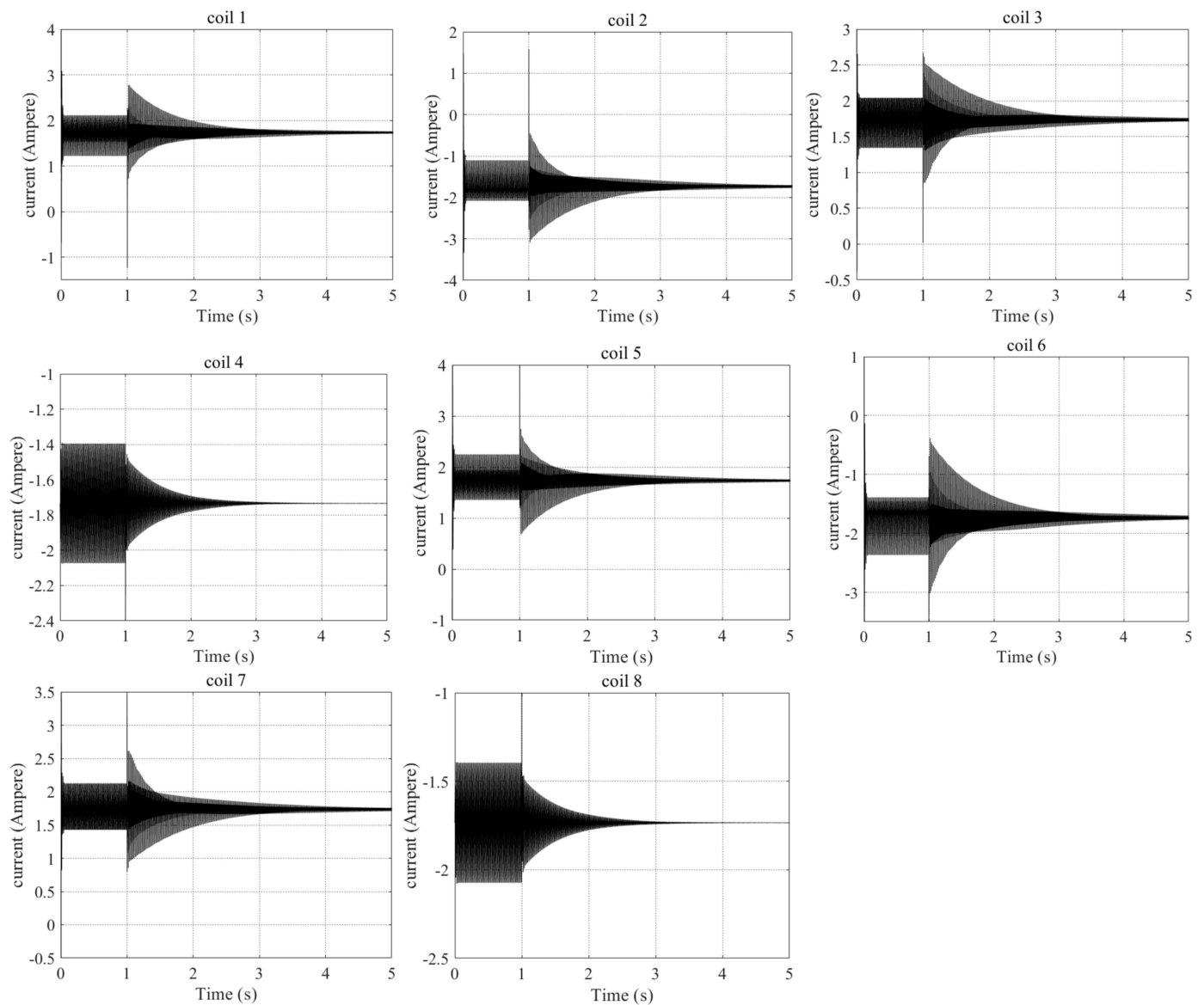


Figure 15. Frequency characteristics of displacement sensor in x-direction.

Table 2. Parameters of mass unbalance and sensor runout.

Parameter	Value	Parameter	Value
$a_{x1}$	41 $\mu\text{m}$	$\phi_{x1}$	$-17.83^\circ$
$a_{x2}$	7.9 $\mu\text{m}$	$\phi_{x2}$	$-52.36^\circ$
$a_{x3}$	5.8 $\mu\text{m}$	$\phi_{x3}$	$-87.28^\circ$
$a_{x4}$	5.7 $\mu\text{m}$	$\phi_{x4}$	$-165.5^\circ$
$a_{x5}$	2.7 $\mu\text{m}$	$\phi_{x5}$	$-192.4^\circ$
$a_{x6}$	3.4 $\mu\text{m}$	$\phi_{x6}$	$-201^\circ$
$\varepsilon$	10 $\mu\text{m}$	$\zeta$	$-17.83^\circ$



**Figure 16.** Transient response of current in each coil with the proposed control strategy.

By analyzing Figure 16, we can draw some conclusions. When the repetitive controllers were applied at 1 s, there was a short magnitude pulse in each coil. However, after the pulse, the current amplitude of each magnetic pole began to decay gradually until zero. Since the two repetitive controllers together determine the current characteristics of each coil and there are strongly coupling characteristics in the magnetic bearing with redundant structures, the frequency-domain characteristics of the entire system changed when the repetitive controllers acted at 1 s, causing the current to oscillate at 1 s, as shown in Figure 16. As shown in Figure 16, at time = 0–1 s, the current amplitude in the coil was approximately  $\pm 0.5$  A. After 1 s, the current amplitude gradually decayed from  $\pm 1$  A to 0 A. It is obvious that the proposed repetitive controllers had a good suppression effect on harmonic current in the redundant magnetic suspension bearing–rotor system. In order to verify that current harmonic suppression could improve the suspended performance of the rotor, the displacements of the rotor in  $x$ - and  $y$ -directions are displayed in Figures 17 and 18, respectively.

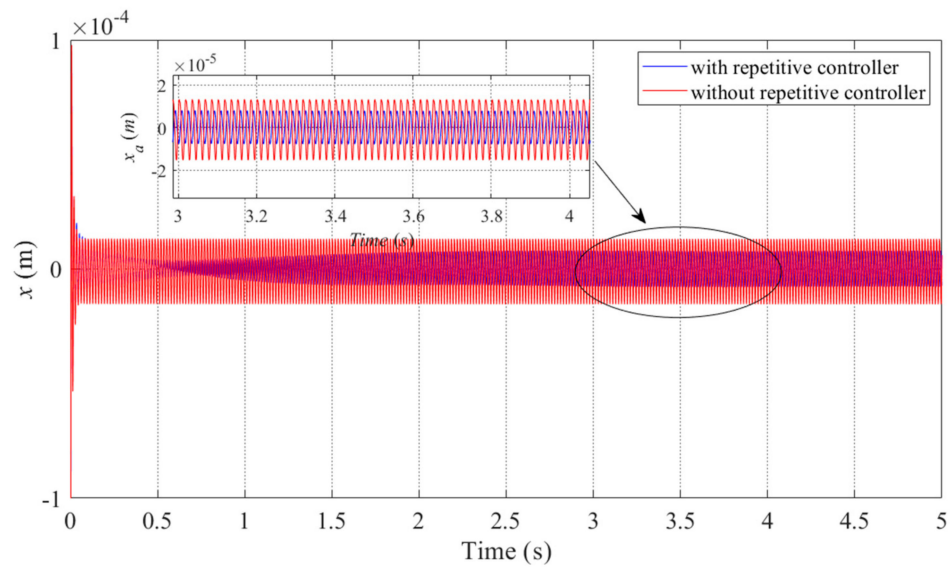


**Figure 17.** Trajectory of the rotor in  $x$ -direction with repetitive control (blue curve) and without repetitive control (red curve).

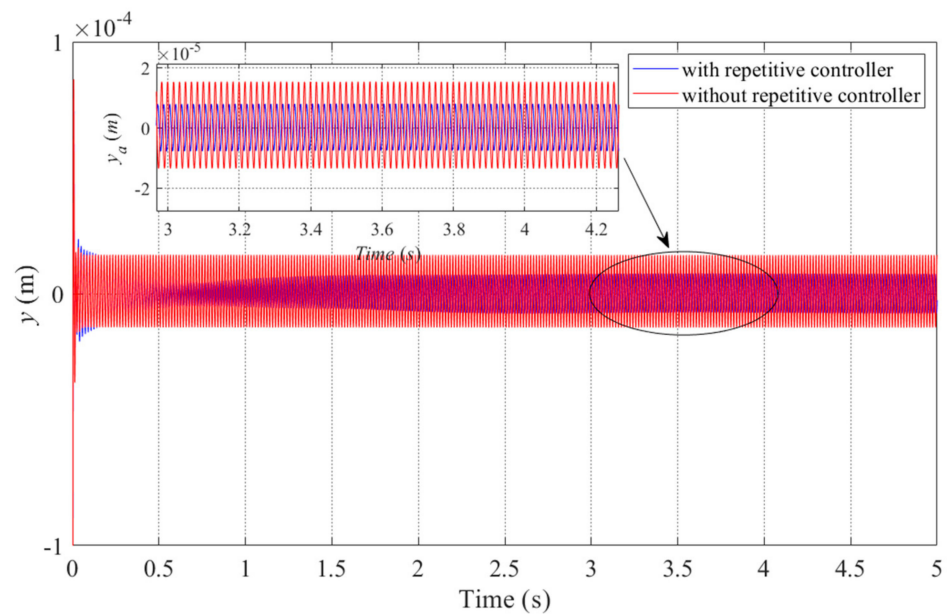


**Figure 18.** Trajectory of the rotor in the  $y$ -direction with repetitive control (blue curve) and without repetitive control (red curve).

For a rotor suspended by a magnetic bearing with redundant structures, Figures 17 and 18 display the displacement of the rotor before and after repetitive control implementation in red and blue, respectively. When repetitive controllers were not applied to the system, the value of  $x$  fluctuated in the range  $\pm 1.6 \times 10^{-5}$  m, and  $y$  fluctuated in the range  $\pm 1.5 \times 10^{-5}$  m. However, for the system which adopted repetitive controllers, the value of  $x$  fluctuated in the range  $\pm 0.5 \times 10^{-5}$  m, and  $y$  fluctuated in the range  $\pm 0.8 \times 10^{-5}$  m. It is obvious that the corresponding amplitudes of  $x$  and  $y$  decreased by about 68.7% and 46.6% when using the proposed control strategy in this paper. However, due to the existence of the unbalanced force of the rotor, the vibration of the rotor could not be completely eliminated, and there was still a vibration of displacement as shown by the blue lines in Figures 17 and 18. Furthermore, a time of about 1 s was needed for the rotor to maintain a stable state after the repetitive controllers were applied to the system.

The simulation results show that the repetitive controllers designed in this paper can be applied to a redundant structure magnetic bearing–rotor system, and the harmonic current of each coil can be effectively suppressed. This allows not only reducing the system’s power consumption but also improving the robustness of the magnetically levitated rotor.

## 5. Conclusions

For a rotor suspended by a heteropolar magnetic bearing with redundant structures, there is disturbance from the mass unbalance and sensor runout in the systems, which causes harmonic currents in the coil. To address this problem, this paper first analyzed the stiffness properties of the magnetic bearing with redundant structures and established the corresponding equivalent closed-loop model. Then, on the basis of the equivalent closed-loop model and the requirements of system stability, a repetitive controller was designed and applied in the magnetic bearing–rotor system with redundant structures. Lastly, the corresponding simulation was carried out, and the numerical results demonstrated that, compared to the case with no repetitive controller in the system, the proposed repetitive controller could effectively suppress the harmonic current of the coils and improve the anti-interference ability of the system. More importantly, by introducing repetitive controllers in the magnetic bearing–rotor system with redundant structures, the rotor suppression accuracy was greatly improved. Additionally, inserting the repetitive controller not only improved the robustness of the magnetically levitated rotor but also reduced the power consumption of the system. However, there are two shortcomings of the repetitive controller proposed in this paper. On the one hand, the response time is long, exceeding 1 s. On the other hand, the repetitive controller requires the exact knowledge of the period of the external signals, and the period is required to be constant. To address these drawbacks of the repetitive controller, we will design improved repetitive control to improve the robustness of the system in future work. Furthermore, when the repetitive control law is applied to the DSP platform for a magnetic bearing, some aspects should be considered. The sampling time must be accurate, and filters should be used to reduce the noise of signal. In particular, the approximate approach can be adopted to realize the phase lead link  $z$  of repetitive control.

**Author Contributions:** Validation, formal analysis, and writing—original draft preparation, B.C.; methodology, X.C.; visualization, S.S.; supervision, R.Z.; visualization, S.D. All authors have read and agreed to the published version of the manuscript.

**Funding:** This work was supported by the Shenzhen Science and Technology Research and Development under Grant JCYJ20190809150603586, the National Key Program of China under Grant No. 2018YFB2000103, and the Fundamental Research Funds for the Central Universities under Grant 2020-YB-022.

**Institutional Review Board Statement:** Not applicable.

**Informed Consent Statement:** Not applicable.

**Data Availability Statement:** Not applicable.

**Conflicts of Interest:** The authors declare no conflict of interest.

## References

1. Allaire, P.E.; Fittro, R.L.; Maslen, E.H.; Wakefield, W.C. Measured Force/Current Relations in Solid Magnetic Thrust Bearings. *J. Eng. Gas Turbines Power* **1997**, *119*, 137–142. [[CrossRef](#)]
2. Keogh, P.; Cole, M.O.T. Dynamics and Control Issues for Fault Tolerance. In *Magnetic Bearings*; Schweitzer, G., Maslen, E.H., Eds.; Springer: Berlin/Heidelberg, Germany, 2009; pp. 407–433.
3. Park, Y. Design and implementation of an electromagnetic levitation system for active magnetic bearing wheels. *IET Control Theory Appl.* **2014**, *8*, 139–148. [[CrossRef](#)]
4. Ren, Y.; Fang, J. High-Precision and Strong-Robustness Control for an MSCMG Based on Modal Separation and Rotation Motion Decoupling Strategy. *IEEE Trans. Ind. Electron.* **2013**, *61*, 1539–1551. [[CrossRef](#)]
5. Cheng, X.; Wang, B.; Chen, Q.; Zhang, L.; Liu, H.; Song, S. A unified design and the current ripple characteristic analysis of digital switching power amplifier in active magnetic-levitated bearings. *Int. J. Appl. Electromagn. Mech.* **2017**, *55*, 391–407. [[CrossRef](#)]

6. Maslen, E.H.; Meeker, D.C. Fault tolerance of magnetic bearings by generalized bias current linearization. *IEEE Trans. Magn.* **1995**, *31*, 2304–2314. [[CrossRef](#)]
7. Na, U.J.; Palazzolo, A. Optimized Realization of Fault-Tolerant Heteropolar Magnetic Bearings. *J. Vib. Acoust.* **2000**, *122*, 209–221. [[CrossRef](#)]
8. Na, U.J.; Palazzolo, A.B.; Provenza, A. Test and Theory Correlation Study for a Flexible Rotor on Fault-Tolerant Magnetic Bearings. *J. Vib. Acoust.* **2002**, *124*, 359–366. [[CrossRef](#)]
9. Noh, M.D.; Cho, S.-R.; Kyung, J.-H.; Ro, S.-K.; Park, J.-K. Design and implementation of a fault-tolerant magnetic bearing system for Tur-bo-Molecular Vacuum Pump. *IEEE-ASME Trans. Mechatron.* **2005**, *10*, 626–631. [[CrossRef](#)]
10. Na, U.J.; Palazzolo, A. Fault tolerance of magnetic bearings with material path reluctances and fringing factors. *IEEE Trans. Magn.* **2000**, *36*, 3939–3946. [[CrossRef](#)]
11. Na, U.J. Fault tolerant control of magnetic bearings with force invariance. *J. Mech. Sci. Technol.* **2005**, *19*, 731–742. [[CrossRef](#)]
12. Na, U.J. Fault tolerant homopolar magnetic bearings with flux invariant control. *J. Mech. Sci. Technol.* **2006**, *20*, 643–651. [[CrossRef](#)]
13. Meeker, D. A Generalized Unbiased Control Strategy for Radial Magnetic Bearings. *Actuators* **2017**, *6*, 1. [[CrossRef](#)]
14. Xin, C.; Baixin, C.; Han, L.; Allen, G.M. An Accurate Linearization of Electromagnetic Force of Heteropolar Magnetic Bearings With Redundant Structures. *J. Eng. Gas Turbines Power* **2020**, *142*, 091002. [[CrossRef](#)]
15. Cheng, B.; Cheng, X.; Song, S.; Deng, S.; Zhou, R.; Hu, Y.; Wu, H. Fault-Tolerant Control of Magnetically-Levitated Rotor with Redundant Structures Based on Improved Generalized Linearized EMFs Model. *Sensors* **2021**, *21*, 5404. [[CrossRef](#)]
16. Meeker, D.; Maslen, E. A Parametric Solution to the Generalized Bias Linearization Problem. *Actuators* **2020**, *9*, 14. [[CrossRef](#)]
17. Cheng, X.; Deng, S.; Cheng, B.; Lu, M.; Zhou, R. Optimization of bias current coefficient in the fault-tolerance of active magnetic bearings based on the redundant structure parameters. *Automatika* **2020**, *61*, 602–613. [[CrossRef](#)]
18. Cheng, X.; Deng, S.; Cheng, B.-X.; Hu, Y.-F.; Wu, H.-C.; Zhou, R.-G. Design and Implementation of a Fault-Tolerant Magnetic Bearing Control System Combined With a Novel Fault-Diagnosis of Actuators. *IEEE Access* **2020**, *9*, 2454–2465. [[CrossRef](#)]
19. Mao, C.; Zhu, C. A real-time variable step size iterative unbalance compensation for active magnetic bearing-rigid rotor systems. *Proc. Chin. Soc. Elect. Eng.* **2018**, *38*, 3960–3968. [[CrossRef](#)]
20. Jian, Z.; Huachun, W.; Weiyu, W.; Kezhen, Y.; Yefa, H.; Xinhua, G.; Chunsheng, S. Online unbalance compensation of a maglev rotor with two active magnetic bearings based on the LMS algorithm and the influence coefficient method. *Mech. Syst. Signal Process.* **2021**, *166*, 108460. [[CrossRef](#)]
21. Cui, P.; Sheng, L.; Zhao, G.; Peng, C. Suppression of Harmonic Current in Active–Passive Magnetically Suspended CMG Using Improved Repetitive Controller. *IEEE/ASME Trans. Mechatron.* **2016**, *21*, 2132–2141. [[CrossRef](#)]
22. Cui, P.; Wang, Q.; Zhang, G.; Gao, Q. Hybrid Fractional Repetitive Control for Magnetically Suspended Rotor Systems. *IEEE Trans. Ind. Electron.* **2017**, *65*, 3491–3498. [[CrossRef](#)]
23. Cai, K.; Deng, Z.; Peng, C.; Li, K. Suppression of Harmonic Vibration in Magnetically Suspended Centrifugal Compressor Using Zero-Phase Odd-Harmonic Repetitive Controller. *IEEE Trans. Ind. Electron.* **2019**, *67*, 7789–7797. [[CrossRef](#)]
24. Cui, P.; Du, L.; Zhou, X.; Li, J.; Li, Y.; Wu, Y. Harmonic vibration moment suppression using hybrid repetitive control for active magnetic bearing system. *J. Vib. Control* **2021**, 1–14. [[CrossRef](#)]
25. Cui, P.; Li, S.; Wang, Q.; Gao, Q.; Cui, J.; Zhang, H. Harmonic Current Suppression of an AMB Rotor System at Variable Rotation Speed Based on Multiple Phase-Shift Notch Filters. *IEEE Trans. Ind. Electron.* **2016**, *63*, 6962–6969. [[CrossRef](#)]
26. He, J.; Peng, C.; Deng, Z.; Zhu, M. Comparison of AMB-rotor system using multiple phase-shift notch filters connected in series and parallel modes for vibration control. In Proceedings of the 2018 Chinese Control And Decision Conference (CCDC), Shenyang, China, 9–11 June 2018; pp. 348–353.
27. Cui, P.; Du, L.; Zhou, X.; Li, J.; Li, Y.; Wu, Y. Harmonic Vibration Control of MSCMG Based on Multisynchronous Rotating Frame Transformation. *IEEE Trans. Ind. Electron.* **2021**, *69*, 1717–1727. [[CrossRef](#)]
28. Jin, C.; Guo, K.; Xu, Y.; Cui, H.; Xu, L. Design of Magnetic Bearing Control System Based on Active Disturbance Rejection Theory. *J. Vib. Acoust.* **2018**, *141*, 011009. [[CrossRef](#)]
29. Ran, S.; Hu, Y.; Wu, H. Design, modeling, and robust control of the flexible rotor to pass the first bending critical speed with active magnetic bearing. *Adv. Mech. Eng.* **2018**, *10*, 1687814018757536. [[CrossRef](#)]
30. Zhang, H.; Liu, J.; Zhu, R.; Chen, H.; Yuan, H. Nonlinear Adaptive Harmonics Vibration Control for Active Magnetic Bearing System With Rotor Unbalance and Sensor Runout. *IEEE Sens. J.* **2021**, *21*, 12245–12254. [[CrossRef](#)]
31. Gallego, G.B.; Rossini, L.; Achtnich, T.; Araujo, D.M.; Perriard, Y. Novel Generalized Notch Filter for Harmonic Vibration Suppression in Magnetic Bearing Systems. *IEEE Trans. Ind. Appl.* **2021**, *57*, 6977–6987. [[CrossRef](#)]
32. Sun, X.; Jin, Z.; Chen, L.; Yang, Z. Disturbance rejection based on iterative learning control with extended state observer for a four-degree-of-freedom hybrid magnetic bearing system. *Mech. Syst. Signal Process.* **2021**, *153*, 107465. [[CrossRef](#)]